ACS APPLIED MATERIALS & INTERFACES

Research Article

www.acsami.org

Novel Cigarlike TiO_2 Nanofibers: Fabrication, Improved Mechanical, and Electrochemical Performances

Jichun You,[†] Wenjia Sheng,[†] Keke Huang,[‡] Changmin Hou,[‡] Huijuan Yue,[‡] Bin Hu,[‡] Min Wang,[§] Donglei Wei,[§] Qingwen Li,[§] Liping Zhao,[†] Wenyong Dong,[†] Zhigang Zhao,*[,§] and Yongjin Li*[,†]

[†]College of Material, Chemistry and Chemical Engineering, Hangzhou Normal University, No. 16 Xuelin Road, Xiasha High-tech Zone, Hangzhou 310036, P.R. China

[‡]State Key Laboratory of Inorganic Synthesis and Preparative Chemistry, College of Chemistry, Jilin University, Changchun 130012, P.R. China

[§]Suzhou Institute of Nanotech and Nanobionics, Chinese Academy of Sciences, 398 Ruoshui Road, Advanced Education District of Dushu Lake, Suzhou Industry Park, Suzhou 215125, P.R. China

S *Supporting Information*

ABSTRACT: By coupling the self-assembly of polystyrene-block-poly(ethylene oxide) (PS-b-PEO) containing titanium precursors with the electrospinning technique, novel cigarlike nanofibers with an outer-shell and inner-continuous-pore structure and resultant fabrics were fabricated. Different from typical porous metal oxides, the prepared high-surface-area nonwoven fabrics show excellent mechanical properties. Not only are these fabrics self-supporting over a large area, but they can also be cut using scissors, which is important for large-scale applications. Furthermore, as electrode materials in Li-ion batteries, these fabrics exhibit much higher charge/discharge capacity and cycle stability compared with the commercially available nanosized TiO_2 (P25). The improved mechanical and electrochemical performances are attributed to the presence of an outer-shell, inner-bicontinuous structures (including continuous TiO_2 frame and continuous nanopores) and hierarchical pores from the cigarlike nanofibers.

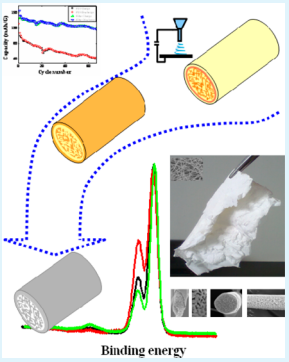

KEYWORDS: *electrospinning, block copolymer, TiO_2, cigarlike, hierarchical porous*

1. INTRODUCTION

Titanium dioxide has captured the interest of scientists and engineers for its applications in areas of photocatalysis, Li-ion batteries, and dye-sensitized solar cells (DSSCs) because of its unique physical and chemical properties.[1−5] The ability to produce this type of material with a high specific surface area is highly desirable for optimizing its efficiency such as in Li-ion batteries.[6] To this end, the strategy of utilizing porosity, especially hierarchical porosity, has been well-established and widely employed. In general, there are two major approaches for fabricating porous structures: "top-down" is well-known as the templating method, whereas "bottom-up" takes advantage of self-assembly.[7] For example, Stein et al. developed the Colloidal Crystal Templating (CCT) method that allows for the formation of three-dimensional porous structures.[8−10] The evaporation-induced self-assembly (EISA) process of block copolymer pioneered by Brinker and his co-workers presented another route for this purpose.[11] A significant number of porous materials with controllable structures and tunable pore sizes are available by the aid of the development of synthetic approaches discussed above. In these reported materials, however, most of the pores are not connected with one another, leading to low performance in many applications.[12−15] In addition, the strategy of fabricating porosity leads to an increase in the specific surface area but also a notable decrease in the mechanical properties. For example, the generalized mixture rule (GMR) results indicate that Young's modulus, hardness and yield strength significantly decrease with increasing porosity.[16,17] As a result, almost all of the reported porous materials are too brittle to be prepared into a self-supporting, large area film or membrane, which significantly limits their applicability.

To simultaneously improve the mechanical properties and specific surface area, we will synthesize novel TiO_2 fibers by a combination of "top-down" and "bottom-up" strategies in this work. Fibers will be prepared by electrospinning a blend solution of polystyrene-block-poly(ethylene oxide) (PS-b-PEO) and titanium tetraisopropoxide (the precursor of TiO_2). Herein, the electrospinning serves as the template (top-down) for generating fibers with diameters ranging from the submicrometer to the micrometer scale, whereas the self-assembly (bottom-up) of PS-b-PEO leads to the micro-structures on the order of several tens of nanometers.[18−20] On the one hand, it is possible to obtain a bicontinuous structure, i.e., a continuous PEO-rich phase containing the TiO_2 precursors and a continuous PS-rich phase in the fibers at

Received: January 23, 2013
Accepted: March 2, 2013
Published: March 2, 2013

   dx.doi.org/10.1021/am4003099 | *ACS Appl. Mater. Interfaces* 2013, 5, 2278−2282

certain volume fraction of the two blocks.[21] On the other hand, one can expect a compact shell-like structure around the surface of the thin fiber due to the spontaneous surface enrichment of one phase in PS-b-PEO, which is caused by a surface energy difference between the two blocks. Upon calcination, novel cigarlike TiO_2 nanofibers with an outer-shell and inner-continuous-pore structure can be fabricated, which will lead to drastically improved mechanical properties and electrochemical performance in Li-ion battery.

2. EXPERIMENTAL SECTION

2.1. Synthesis Procedure. The procedure used to fabricate TiO_2 nanofibers is provided in Scheme 1. Polystyrene-block-poly(ethylene oxide) ($M_w \approx$ 59000-b-31000, PDI $\approx$ 1.05, purchased from Aldrich) and titanium-tetraisopropoxide mixed at a 1/2 weight ratio in chloroform (0.3 g/mL) and stirred for 10 h. The polymer solution was electrospun from a 5 mL syringe with at a feeding rate of 0.4 mL/h by a syringe pump (KDS 200, KD Scientific, USA) by applying a 12−15 kV voltage to the needle. The as-spun fibers were collected by a collector, i.e., a copper-plate electrode covered with a polished silicon wafer, which was placed 10−15 cm away from the needle. As-spun fibers were annealed at 120 °C for 48 h in vacuum, followed by calcinations at 450 °C for 2 h to remove PS-b-PEO.

Scheme 1. Fabrication of TiO_2 Fibers Prepared by Electrospinning a Blend Solution of Polystyrene-block-poly(ethylene oxide) (PS-b-PEO) and Titanium-tetraisopropoxide

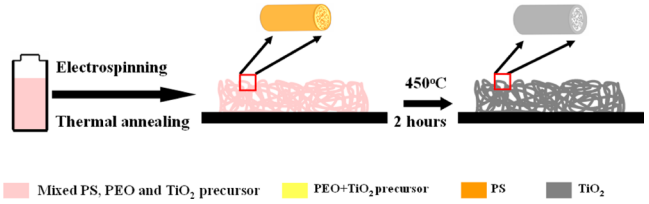

2.2. Characterization. A Hitachi S-4800 Field Emission Scanning Electron Microscopy (FESEM) was used for morphology measurements at an accelerating voltage of 5.0 KV. EDX measurement was performed at accelerating voltages of 0−8KeV. FEI Tecnai G2 F20 s-twin D573 transmission electron microscope (TEM) was employed at operated at 200 kV. A HELIOS NanoLab 600i (FEI, USA) Focused Ion Beam (FIB) that provides 30 keV Ga+ ion beam with intensities ranging from 1 pA to 30 pA was adopted to "cut" and scan profile and surface of fibers. The XRD data were collected from 2θ = 5−80° at a scanning speed of 2°/min with a step interval of 0.02°. The instrument (XRD, Bruker-D8) was operated at a 35 kV voltage and 30 mA current. Surface chemical composition of the films was determined on a Thermo ESCALAB 250 X-ray photoelectron spectrometer (XPS) using monochromatic Al X-ray source (1486.6 eV). The binding energy peaks were charge-referenced to the C−C/C−H peak at 284.6 eV. The thermal behaviors of as-spun fibers were measured under N_2 using a thermogravimetric analyzer (TGA, TA-Q2000) with increasing temperature from 30 to 950 °C by 10 K/min. Differential scanning calorimetry (DSC) was performed (DSC, TA-Q2000) at variable heating (or cooling) rates as well as at isothermal conditions. Before sample scan, the heat flow and temperature were calibrated with sapphires and pure indium, respectively.

The surface area was measured using Brunauer−Emmet−Teller (BET) method using nitrogen adsorption at 77 K. The Barret−Joyner−Halenda (BJH) method was used to obtain pore size distribution of TiO_2 nanofiber. The samples were degassed at 300 °C for 2 h before the measurements. The as-prepared TiO_2 nanofiber, acetylene black, and binder (PVDF) were mixed together homogeneously in a weight ratio of 4:1:1. After being blended in several drops of N-methylpymolidinone (NMP), the mixture was spread uniformly on a 10-μm thick copper foil with a diameter of 18 mm. The electrodes were dried in an oven at 120 °C for 20 h. The electrolyte used was 1 M LiPF6 dissolved in the mixture of ethyl carbonate (EC) and dimethyl carbonate (DMC) with the volume ratio of 1:1. The coin cells were assembled in an argon-filled glovebox. With a Voltalab PGP 201 cell test system (Radiometer analytical, Copenhagen), the discharge/charge measurements were taken at 36 and 360 mA g^{-1} with cutoff voltages of 2.7 and 1.0 V.

3. RESULTS AND DISCUSSION

Figure 1 illustrates the scanning electron microscope (SEM) images of the as-spun and as-annealed fibers. It is clear that we can obtain uniform nanofibers by coupling the self-assembly of PS-b-PEO containing titanium precursors with the electrospinning technique. The diameter of these fibers can be varied from 150 to 900 nm by tuning the electrospinning parameters such as the concentration of blend solution, spinning voltage and distance between the needle and the collector. Calcination at 450 °C for 2 h leads to a weight loss of 68%, as determined by thermogravimetric analysis (TGA) in Figure S1 in the Supporting Information, which is caused by the degradation of the polymer and the transition from titanium tetraisopropoxide to titanium dioxide. Energy-dispersive X-ray (EDX) spectrum of the scanned area indicates only the presence of Ti and O elements in the sample, confirming the complete degradation of PS-b-PEO (see Figure S2 in the Supporting Information). To investigate the structure formation and evolution in detail, X-ray photoelectron spectroscopy (XPS) measurements were performed to examine the surface composition and the results are displayed in Figure 2. There are three peaks at 284.6, 286.4, and 291.3 eV corresponding to C−C, C−O−C in PEO, and the aromatic $\pi-\pi^*$ shakeup in PS, respectively.[22,23] There is a stronger peak at 286.4 eV in the as-spun fibers compared with

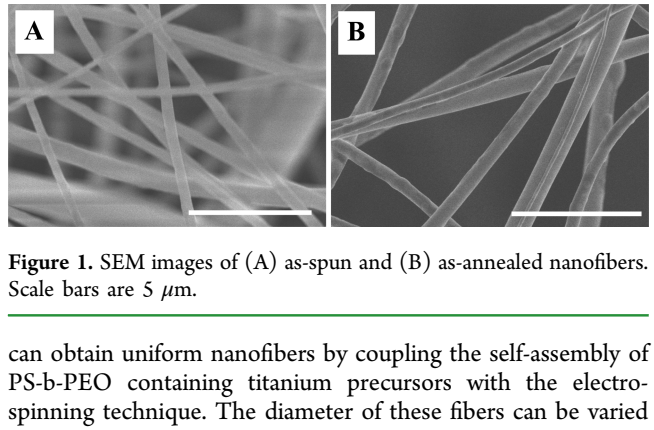

Figure 1. SEM images of (A) as-spun and (B) as-annealed nanofibers. Scale bars are 5 μm.

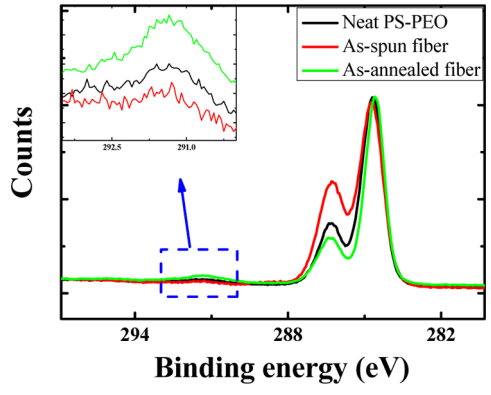

Figure 2. C1s region of the XPS spectra of neat PS-PEO, as-spun (with TiO_2 precursors) and as-annealed (with TiO_2 precursors) fibers. Inset is local enlargement part of the spectra.

that of neat PS-PEO, indicating that more PEO-rich phases are on the fiber surface. Annealing at 120 °C for 48 h leads to the noticeable intensity decrease of this peak, which is caused by the increase of PS-rich phase (i.e., the decrease of PEO-rich phase). Then, we can describe the formation of the cigarlike structures in the following manner: due to its higher solubility in chloroform compared with PS, PEO tends to remain in solution longer during the electrospinning process, which results in an excess of the PEO-rich phase on the surface of fibers. As a consequence of the covalent-bond between the two blocks,[24,25] this PEO-rich phase is accompanied by a neighboring PEO dissipated layer, i.e., PS-rich layer. Annealing at 120 °C, above glass transition temperature of both PS and PEO, leads to a surface enrichment of PS block due to its lower surface free energy relative to PEO.[26,27] This assessment is supported by the evolution of the peak at 291.3 eV, that is to say, the increase of peak intensity upon annealing. Concurrently, the microphase separation produces bicontinuous structures of PS-rich and PEO-rich phases inside the fibers. During the whole process described above, the PEO phase is accompanied by the TiO_2 precursors,[28] which can be validated by differential scanning calorimetry (DSC) result. In Figure 3,

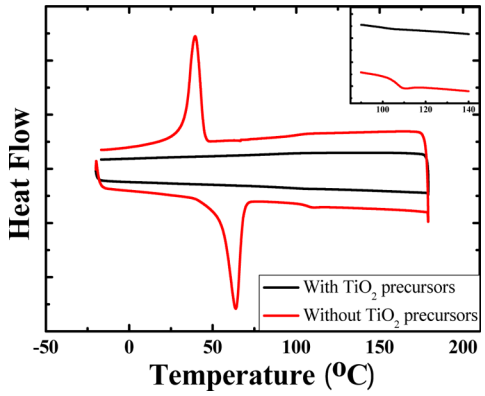

Figure 3. A typical DSC scan for as-spun fibers with and without TiO_2 precursors. Inset is local enlargement part of the spectra.

the sharp and obvious peaks (at ~39 °C in cooling and ~63 °C in heating process) in red line represent the crystallization and melting of PEO-rich phase. Glass transition of PS-rich phase (at ~107 °C) is also clear due to the poor miscibility of PS and PEO. In the black curve, however, crystallization and melting peak of PEO disappears, whereas the glass transition peak of PS is still observed. This result indicates that TiO_2 precursors swell PEO domains and suppress their crystallization and subsequent melting, but have no remarkable effect on the glass transition of PS. Namely, TiO_2 precursors have better miscibility with PEO (relative to PS) before calcinations. Therefore, there are complex structures in the nanofibers before calcination, that is, PS shell accompanied by PEO sublayer (with TiO_2 precursors) and microphase separated PS and PEO (with TiO_2 precursors) domains in the fibers. Upon calcinations on 450 °C for 2 h, PS block is removed as well as PEO block. Then, titanium tetraisopropoxide, with the same distribution with PEO before calcination, is transferred into titanium dioxide and exposed as the "new" shell. Furthermore, nanopores resulted from the degradation of PS and continuous TiO_2 from PEO can be obtained inside the shell of fibers. Consequently, the migration of PS and PEO, better miscibility between TiO_2 precursors with PEO and microphase separation in block copolymer produce fibers with novel cigarlike structures shown in Figure 4. Both the SEM images (Figure

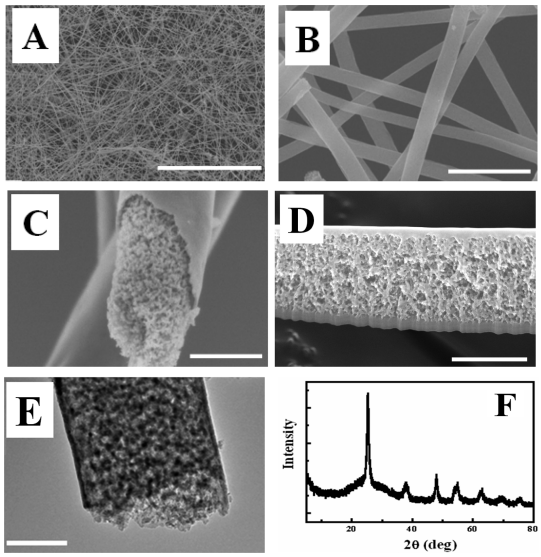

Figure 4. (A–D) SEM and (E) TEM images and (F) XRD of TiO_2 fibers prepared by electrospinning. Scale bars are 5 μm, 2000, 500, 400, and 200 nm in A–E, respectively.

4A–D) and the transmission electron microscope (TEM) image (Figure 4E) of a nanofiber demonstrate that the calcinated TiO_2 fibers have an inner bicontinuous structure (including continuous TiO_2 and continuous pores) and a compact shell around the fibers. The size of the bicontinuous structure (~30 nm) is close to the size of the microphase separated domains in the bulky PS-b-PEO. The thickness of fiber shell is ~40 nm, as determined by TEM.[29,30] In addition, the X-ray diffraction (XRD) pattern of nanofibers obtained by electrospinning is provided in Figure 4F, and reveals strong diffraction peaks at 25, 38, and 48°. This result indicates that the TiO_2 is in the anatase phase.[31,32] Furthermore, this novel structure can be validated by SEM images along the radial and axial directions (cut by FIB). These images present an excellent juncture between the outer-shell and inner-continuous TiO_2, reconfirming the absence of the PS-rich phase in neighboring layer of gyroid in fibers prior to calcination (Figure S3). This is in good agreement with XPS result.

We note the synergism between the copolymer and the inorganic material that allows for the formation of the cigarlike structure: the PS-b-PEO serves as the medium for the TiO_2 precursor during the electrospinning, whereas the latter acts as the backbone that maintains the shape of the fibers during annealing at 120 °C (Figure 1). As shown in Figure S4 in the Supporting Information, upon annealing, the fibers prepared without the TiO_2 precursor become droplets because of the poor thermal stability of the neat PS-b-PEO fibers and its poor wettability on the silicon wafer.[33] Therefore, the presence of a block copolymer provides a medium for the electrospinning process, a template for the cigar, and a possible structure- and size- controlling agent (including the gyroid inside and the shell around the fiber surface, we will discuss the structure control in our further publications), whereas the TiO_2 precursor provides control over the shape of the fiber during the annealing and calcination processes.

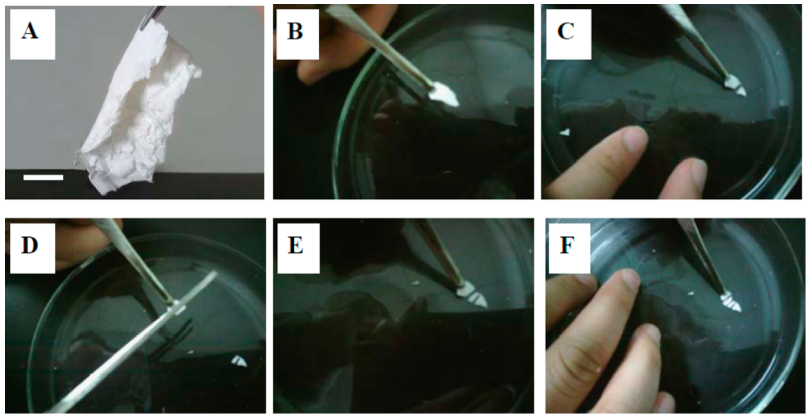

Figure 5. Photos of fabrics from TiO_2 fibers trimmed by scissors. Scale bar in A is 0.5 cm.

To investigate the pore size distribution of the obtained fibers, N_2 adsorption isothermal tests were performed using the Brunauer–Emmett–Teller (BET) and Barrett–Joyner–Halenda (BJH) techniques. The specific surface area and pore volume were determined to be 384 m^2 g^{-1} and 0.64 cm^3 g^{-1}, respectively. Figure S5 in the Supporting Information demonstrates the existence of pores resulting from both the removal of the PS-rich phase in microphase separated bicontinuous structures and the voids among individual fibers.[34] Furthermore, the pore size is predominantly distributed between 10 to 430 nm with two peaks at 32 and 300 nm, indicating the presence of hierarchical pores in the fabricated materials. This is in accord with the SEM (Figure 4A, B, corresponding to submicrometer scale pores among fibers) and TEM (Figure 4E corresponding to ~30 nm scale pores in fibers) results.

In general, the mechanical properties decrease with increasing pore density and volume. A positive effect is expected due to the formation of a shell around the fiber and the presence of a continuous TiO_2 frame in the cigarlike structures. In this work, therefore, large-area nonwoven fabric from TiO_2 fibers, which can be easily obtained after calcinations, presents exceptional mechanical performance (Figure 5A). All nonwoven fabrics are self-supporting over a large area and can be easily handled. Moreover, it is exciting that fabrics from cigarlike nanofibers can be cut using a scissors and reverted to their original shape by putting trimmed pieces together (shown in Figure 5B–F). According to the above results, the presence of a fiber shell and a continuous TiO_2 frame inside the fiber do increase the strength and toughness of our fabrics remarkably.

Nanostructured TiO_2 has been used as an electrode for Li-ion batteries due to its excellent properties including safety against overcharging, chemical stability and low production cost.[35−40] Herein, panels A and B in Figure 6 provide a comparison between the charge/discharge curves of commercial nanoparticles (P25) and cigarlike TiO_2 nanofibers in a Li-ion battery, respectively.[36] Plateaus are observed at approximately 1.76 V (discharge process) and 1.90 V (charge process) for both curves at a constant current rate of C/10. The first cycle discharge capacity and the corresponding charge capacity for our fibers are 336 and 208 mA h g^{-1}, respectively, which are similar to the values obtained for P25. From the second cycle on, both discharge and charge capacity in our fibers has a higher value compared to P25. Furthermore, the change in the specific charge/discharge capacity as a function of the cycle number at a

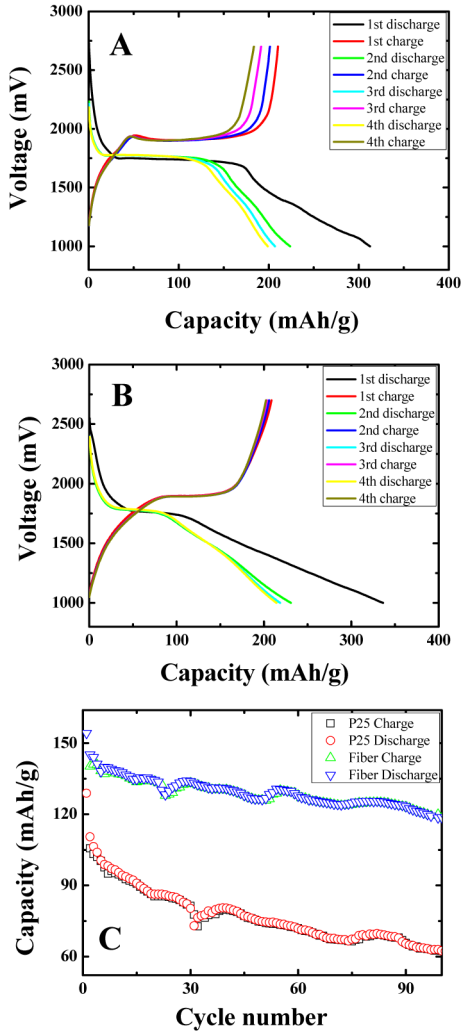

Figure 6. Early stage of charge/discharge of (A) P25, (B) nonwoven fabrics from cigarlike TiO_2 fibers, and (C) discharge capacity as a function of cycle number.

constant current density (1C) is shown in Figure 6C. On the one hand, the charge/discharge capacity of nanofibers is much higher than that of P25. On the other hand, the decrease in the capacity after 100 charge/discharge cycles is approximately 22% for the nanofibers exhibit improved performance in both charge/discharge capacity and cycling stability in comparison

dx.doi.org/10.1021/am4003099 | ACS Appl. Mater. Interfaces 2013, 5, 2278−2282

with P25, which are important parameters for Li-ion batteries. It is reasonable to attribute these improvements to the enhancement of the specific surface area and pore volume, which create connected and accessible pores for Li ions in the bicontinuous structures resulting from the microphase separation.

4. CONCLUSION

In summary, the electrospinning of a blend solution of block copolymer and TiO_2 precursor is a feasible method for fabricating hierarchically porous materials with a combination of "top-down" and "bottom-up" strategies. Nanofibers prepared using this approach exhibit a novel cigarlike structure with an outer-shell and inner-continuous pore. Surface enrichment resulting from selective migration of them during the electrospinning and the subsequent thermal annealing process account for the formation outer-shell. On the other hand, microphase separation of PS-b-PEO in the confined geometry environment is response for the inner-bicontinuous structures including continuous TiO_2 frame and continuous pores. Furthermore, fabrics from these nanofibers exhibit improved mechanical properties and enhanced performance in Li-ion batteries in comparison with P25 as expected. Existence of outer-shell and inner-bincontinuous structures plays a key role in these improvements. Our results not only serve as an important starting point for generating a connected, hierarchically porous material with control over the structure but also provide the possibility for mass production in view of the widespread application of electrospinning on the industrial scale.

■ ASSOCIATED CONTENT

Supporting Information

Figure S1−S5. This material is available free of charge via the Internet at http://pubs.acs.org.

■ AUTHOR INFORMATION

Corresponding Author

*E-mail: yongjin-li@hznu.edu.cn (Y.J.L.); zgzhao2011@sinano.ac.cn (Z.G.Z.).

Notes

The authors declare no competing financial interest.

■ ACKNOWLEDGMENTS

This work was financially supported by the National Science Foundation of China (21074029, 51173036, 21104013, 21104014, and 51102274), Zhejiang Provincial Natural Science Foundation of China (R4110021), and PCSIRT (IRT 1231).

■ REFERENCES

(1) Linsebigler, A. L.; Lu, G.; Yates, J. T. *Chem. Rev.* **1995**, *95*, 735−758.
(2) Seo, Y. G.; Woo, K.; Kim, J.; Lee, H.; Lee, W. *Adv. Funct. Mater.* **2011**, *21*, 3094−3103.
(3) Park, J. T.; Patel, R.; Jeon, H.; Kim, D. J.; Shin, J.; Kim, J. H. *J. Mater. Chem.* **2012**, *22*, 6131−6138.
(4) Chen, X.; Liu, L.; Yu, P. Y.; Mao, S. S. *Science* **2011**, *331*, 746−750.
(5) Liu, B.; Aydil, E. S. *J. Am. Chem. Soc.* **2009**, *131*, 3985−3990.
(6) Wang, Y. Q.; Gu, L.; Guo, Y. G.; Li, H.; He, X. Q.; Tsukimoto, S.; Ikuhara, Y.; Wan, L. J. *J. Am. Chem. Soc.* **2012**, *134*, 7874−7879.
(7) Liu, Z.; Li, Y.; Zhao, Z.; Cui, Y.; Hara, K.; Miyauchi, M. *J. Mater. Chem.* **2010**, *20*, 492−497.
(8) Stein, A.; Li, F.; Denny, N. R. *Chem. Mater.* **2008**, *20*, 649−666.
(9) Vu, A.; Stein, A. *Chem. Mater.* **2011**, *23*, 3237−3245.
(10) Stein, A.; Wang, Z.; Fierke, M. A. *Adv. Mater.* **2009**, *21*, 265−293.
(11) Brinker, C. J.; Lu, Y.; Sellinger, A.; Fan, H. *Adv. Mater.* **1999**, *11*, 579−585.
(12) Yin, Y.; Xia, Y. *Adv. Mater.* **2001**, *13*, 267−271.
(13) Manoharan, V. N.; Elsesser, M. T.; Pine, D. J. *Science* **2003**, *301*, 483−487.
(14) Hoogenboom, J. P.; Rétif, C.; de Bres, E.; van de Boer, M.; van Langen-Suurling, A. K.; Romijn, J.; van Blaaderen, A. *Nano Lett.* **2004**, *4*, 205−208.
(15) Leunissen, M. E.; Christova, C. G.; Hynninen, A. P.; Royall, C. P.; Campbell, A. I. *Nature* **2005**, *437*, 235−240.
(16) Wang, D.; Möhwald, H. *J. Mater. Chem.* **2004**, *14*, 459−468.
(17) Ji, S.; Gu, Q.; Xia, B. *J. Mater. Sci.* **2006**, *41*, 1757−1768.
(18) Cheng, J. Y.; Ross, C. A.; Smith, H. I.; Thomas, E. L. *Adv. Mater.* **2006**, *18*, 2505−2521.
(19) Pradeep, C. P.; Long, D. L.; Streb, C.; Cronin, L. *J. Am. Chem. Soc.* **2008**, *130*, 14946−14947.
(20) Li, D.; Xia, Y. *Adv. Mater.* **2004**, *16*, 1151−1170.
(21) Kim, I.; Wakada, T.; Akasaka, S.; Nishitsuji, S.; Saijo, K.; Hasegawa, H.; Ito, K.; Takenaka, M. *Macromolecules* **2009**, *42*, 5266−5271.
(22) Guo, S.; Shen, L.; Feng, L. *Polymer* **2001**, *42*, 1017−1022.
(23) Ton-That, C.; Shard, A. G.; Daley, R.; Bradley, R.H.. *Macromolecules* **2000**, *33*, 8453−8459.
(24) Adams, D. J.; Butler, M. F.; Weaver, A. C. *Langmuir* **2006**, *22*, 4534−4540.
(25) You, J.; Shi, T.; Liao, Y.; Li, X.; Su, Z.; An, L. *Polymer* **2008**, *49*, 4456−4461.
(26) Van, O. C. J.; Chaudhury, M. K.; Good, R. J. *Adv. Colloid Interface Sci.* **1987**, *28*, 35−64.
(27) Wu, S. *J. Macromol. Sci.* **1974**, *C10*, 1.
(28) Cha, M. A.; Shin, C.; Kannaiyan, D.; Jang, Y. H.; Kochuveedu, S. T.; Ryu, D. Y.; Kim, D. H. *J. Mater. Chem.* **2009**, *19*, 7245−7250.
(29) Mansky, P.; Tsui, O, K, C.; Russell, T. P. *Macromolecules* **1999**, *32*, 4832−4837.
(30) Li, L.; Séréro, Y.; Koch, M. H. J.; de Jeu, W. H. *Macromolecules* **2003**, *36*, 529−532.
(31) Kang, X.; Chen, S. *J. Mater. Sci.* **2010**, *45*, 2696−2702.
(32) Liu, X.; Zhou, W.; Yin, Z.; Hao, X.; Wu, Y.; Xu, X. *J. Mater. Chem.* **2012**, *22*, 3916−3921.
(33) Neto, C.; James, M.; Telford, A. M. *Macromolecules* **2009**, *42*, 4801−4808.
(34) Rouquerol, J.; Avnir, D.; Fairbridge, C. W.; Everett, D. H.; Haynes, J. M.; Pernicone, N.; Ramsay, J. D. F.; Sing, K. S. W.; Unger, K. K. *Pure Appl. Chem.* **1994**, *66*, 1739−1758.
(35) Yang, M. C.; Lee, Y. Y.; Xu, B.; Powers, K.; Meng, Y. S. *J. Power Sources* **2012**, *207*, 166−172.
(36) Subramanian, V.; Karki, A.; Gnanasekar, K. I.; Eddy, F. P.; Rambabu, B. *J. Power Sources* **2006**, *159*, 186−192.
(37) Linsebigler, A. L.; Lu, G.; Yates, J. T. *Chem. Rev.* **1995**, *95*, 735−758.
(38) Wang, D.; Choi, D.; Li, J.; Yang, Z.; Nie, Z.; Kou, R.; Hu, D.; Wang, C.; Saraf, L. V.; Zhang, J.; Aksay, I. A.; Liu, J. *ACS Nano* **2009**, *3*, 907−914.
(39) Wang, J.; Zhou, Y.; Hu, Y.; O'Hayre, R.; Shao, Z. *J. Phys. Chem. C* **2011**, *115*, 2529−2536.
(40) Armstrong, G.; Armstrong, A. R.; Bruce, P. G.; Reale, P.; Scrosati, B. *Adv. Mater.* **2006**, *18*, 2597−2600.